drag force on the motion of non-Newtonian liquid across a stretching surface can be view in Ref. [22, 23].

The phenomenon of non-uniform heat sink/source has familiar solicitations in medicine and many engineering activities like cooling of metallic sheets, the intention of a thrust bearing, unpolished oil retrieval, etc. Tawade et al. [24] elucidated the magnetohydrodynamic time-dependent thin film motion and heat transport across a stretched sheet in the attendance of uneven heat sink/source. It was clinched that uneven heat parameters play an essential role in heat transfer performance. The flow and heat transport features of non-Newtonian nanoliquid film flow across an unsteady stretching sheet were reported by Zhang et al. [25]. Thumma et al. [26] reported the variable heat sink or source on MHD convection motion of nanoliquid owing to stretching of a sheet. Familiar Keller-Box numerical procedure is exploited to get the solution. Impact of uneven thermal sink/source on an electrically conducting shear thickening liquid flow across a variable thickness sheet was explored by Ramadevi et al. [27]. Animasaun et al. [28] scrutinized the heat transfer features on time-dependent motion of an electrically accompanying nanoliquid due to stretching of a surface in the presence of Hall effects.

In all the afore investigations, researchers scrutinized the heat transfer and flow features of either shear thickening or Newtonian liquids over solid geometry with physical attributes. The purpose of the current investigation is to give numerical exploration of time-dependent magnetohydrodynamic thin film flow of hybrid ferrofluid past, an elongated surface in the attendance of irregular heat source/sink. A keen investigation is performed and observed the significant change in the momentum and thermal transfer nature of the ferro- and hybrid ferroliquid.

Formulation

Water-ethylene glycol-based ferro- and hybrid ferrofluid past an elongated sheet is considered in the (x,y) coordinate system as displayed in Fig. 1. Here, the stretched sheet with velocity $u_{\rm w}=bx/(1-\alpha t)$ is measured along x-axis, where b,α are constants and y-axis is perpendicular to it. $T_{\rm w}=T_0-T_{\rm r}(bx^2/2v_{\rm f}\sqrt{(1-\alpha t)})$ is the temperature near the wall, where $T_{\rm r},T_0$ are the reference and slit temperatures. A time-dependent magnetic field $B=B_0(1-\alpha t)^{-0.5}$ is considered. Irregular heat source/sink and thermal radiation effects take into consideration. It is supposed that no slip occurs between ferrous particles.

With the afore taken assumptions, the flow equations are given by

Equation of continuity

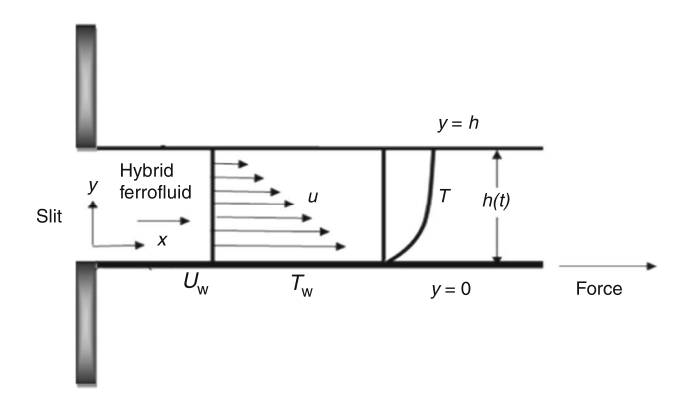


Fig. 1 Flow configuration

$$\frac{\partial u}{\partial x} + \frac{\partial v}{\partial y} = 0,\tag{1}$$

Equation of momentum

$$\rho_{\rm hnf}\left(\frac{\partial u}{\partial t} + u\frac{\partial u}{\partial x} + v\frac{\partial u}{\partial y}\right) = \mu_{\rm hnf}\frac{\partial^2 u}{\partial y^2} + \sigma_{\rm hnf}B^2u,\tag{2}$$

Energy equation

$$(\rho c_{\rm p})_{\rm hnf} \left(\frac{\partial T}{\partial t} + u \frac{\partial T}{\partial x} + v \frac{\partial T}{\partial y} \right) = \left(k_{\rm hnf} + \frac{16T_{\infty}^3 \sigma^*}{3k^*} \right) \frac{\partial^2 T}{\partial y^2} + q''', \tag{3}$$

For the designed problem, the boundary conditions are taken as

$$u = u_{w}, v = 0, T = T_{w} \text{ at } y = 0,$$

 $\frac{\partial u}{\partial y} = \frac{\partial T}{\partial y} = 0 \text{ at } y = h, \quad v = \frac{\partial h}{\partial t} \text{ at } y = h(t),$

$$(4)$$

where σ^* is the Stefan–Boltzmann constant, k^* constant of mean absorption, and h(t) is the film thickness.

The non-uniform heat source/sink q''' is given by

$$q''' = \frac{k_{\rm f} u_{\rm w} (T_{\rm w} - T_0)}{x v_{\rm f}} \left(A^* f' + B^* \frac{(T - T_0)}{(T_{\rm w} - T_0)} \right),\tag{5}$$

Here, the increasing and decreasing values of A^* and B^* correspond to internal heat source/sink, respectively.

The hybrid nanofluid parameters are given as

$$\begin{aligned} &(\rho c_{p})_{hnf} = (1-\phi)(\rho c_{p})_{f} + \phi_{1s}(\rho c_{p})_{1s} + \phi_{2s}(\rho c_{p})_{2s}, \\ &\frac{k_{hnf}}{k_{f}} = \frac{k_{1s} + k_{2s} + 2(1-\phi)k_{f} + 2\phi_{1s}k_{1s} + 2\phi_{2s}k_{2s}}{k_{1s} + k_{2s} + (2+\phi)k_{f} - \phi_{1}k_{1s} - \phi_{2}k_{2s}}, \\ &\mu_{hnf} = \frac{\mu_{f}}{(1-\phi)^{2.5}}, \ \phi = \phi_{1s} + \phi_{2s}, \ \rho_{hnf} = (1-\phi)\rho_{f} + \phi_{1s}\rho_{1s} + \phi_{2s}\rho_{2s}, \\ &\frac{\sigma_{hnf}}{\sigma_{f}} = \left[1 + \frac{3\left(\frac{\sigma_{1s}\phi_{1s} + \sigma_{2s}\phi_{2s}}{\sigma_{f}}\right) - 3\phi}{\left(\frac{\sigma_{1s} + \sigma_{2s}}{\sigma_{f}}\right) + 2 - \left(\frac{\sigma_{1s}\phi_{1s} + \sigma_{2s}\phi_{2s}}{\sigma_{f}}\right) + \phi}\right], \end{aligned}$$



2148 K. Anantha Kumar et al.

Table 1 Thermo-physical properties

Thermo-physical properties	Water + EG 50%	Fe_3O_4	CoFe ₂ O ₄
ρ /kg m ⁻³	1056	5180	4907
C_p /J kg ⁻¹ K ⁻¹ k/W m ⁻¹ K ⁻¹	3288	670	700
$k/W \text{ m}^{-1} \text{ K}^{-1}$	0.425	9.7	3.7
σ /S m ⁻¹	0.00509	0.74×10^6	1.1×10^{7}
Pr	29.86	_	-

where ϕ is the volume fraction of hybrid ferroparticles, ϕ_1, ϕ_2 indicates the volume fraction of the individual ferroparticles. Here, the suffixes hnf, f and s specify the hybrid ferrofluid, base fluid, and solid particles.

The similarities are adopted for the given problem as

$$\eta = \frac{1}{\beta} \left(\frac{b}{v_{\rm f}(1 - \alpha t)} \right)^{0.5} y, \ \psi = \beta \left(\frac{v_{\rm f}b}{(1 - \alpha t)} \right)^{0.5} x f(\eta), \ \theta = \frac{(T - T_0)}{(T_{\rm w} - T_0)},
u = \frac{\partial \psi}{\partial y}, \ v = -\frac{\partial \psi}{\partial x}, \ T_{\rm w} = T_0 - T_{\rm r}(bx^2/2v_{\rm f})(1 - \alpha t)^{-1.5}\theta(\eta),$$
(7)

Using Eqs. (5) and (7), the Eqs. (2) and (3) can be transformed as

$$\frac{\mu_{\rm hnf}}{\mu_{\rm f}}f''' + \frac{\rho_{\rm hnf}}{\rho_{\rm f}}\lambda\left(f'' - (f')^2 - Sf' - S\frac{\eta}{2}f''\right) - M\frac{\sigma_{\rm hnf}}{\sigma_{\rm f}}f' = 0, \tag{8}$$

$$\left(\frac{k_{\rm hnf}}{k_{\rm f}} + \frac{4}{3}R\right)\theta'' - Pr\frac{(\rho c_{\rm p})_{\rm hnf}}{(\rho c_{\rm p})_{\rm f}}\lambda\left(\frac{S}{2}(3\theta + \eta\theta') + 2\frac{\partial f}{\partial \eta}\theta - f\theta'\right) + B^*\theta + A^*\frac{\partial f}{\partial \eta} = 0,$$
(9)

with the conditions

$$f(\eta) = 0, f'(\eta) = 1, \ \theta(\eta) = 1, \ \text{at } \eta = 0,$$

$$f(\eta) = S/2, f''(\eta) = 0, \ \theta'(\eta) = 0, \ \text{at } \eta = 1,$$
(10)

In Eqs. (8)–(10), the non-dimensional parameters (Prandtl number (Pr), magnetic field parameter (M), radiation parameter (R), unsteadiness parameter (S), and film thickness parameter (λ) can be defined as

$$Pr = \frac{v_{\rm f}}{\alpha_{\rm f}}, \ M = \frac{\sigma_{\rm f} B_0^2}{b\rho_{\rm f}}, \ R = \frac{4\sigma^* T_0^3}{k^* k_{\rm f}}, \ S = \frac{\alpha}{b}, \ \lambda = \beta^2,$$
 (11)

The reduced Nusselt number Nu_x is given by

$$Re_{x}^{-0.5}Nu_{x} = -\frac{1}{\beta}\left(\frac{k_{\text{hnf}}}{k_{\text{f}}} + \frac{4}{3}R\right)\theta'(0),$$
 (12)

where $Re_{\rm x} = \frac{u_{\rm w}x}{v_{\rm f}}$ is the Reynolds number.

Table 2 Validation of the results for $-\theta'(0)$ when $R=M=\phi=0$ and Pr=1

S	Xu et al. [8]	Sandeep [16]	Present results
1.0	2.67722	2.67722	2.67721
1.2	1.99959	1.99959	1.99959
1.4	1.44775	1.44775	1.44774
1.6	0.95669	0.95669	0.95669
1.8	0.48453	0.48453	0.48453

Discussion of results

The nonlinear ordinary differential Eqs. (8) and (9) with the corresponding boundary conditions Eq. (10) have been resolved numerically by fourth-order Runge-Kutta-based shooting method. Further, the physical behavior of the involved parameters on the distributions of velocity and temperature was examined. We allocated the values for the flow parameters as M = 3, S = 0.5, $\lambda = 0.5$ $A^* = B^* = 0.5$, an R = 1. For the entire study, these values are taken constant apart from the variable values as shown in the graphs and tables. In the entire discussion, $f'(\eta)$ and $\theta(\eta)$ represent the distributions of velocity and temperature. The thermo-physical properties of water + EG (50-50%), Fe₃O₄, and CoFe₂O₄ are shown in Table 1. In this examination, solid lines symbolize the ferrofluid (water + EG + Fe₃O₄) and dashed lines symbolize the hybrid ferrofluid (water $+ EG + Fe_3O_4 + CoFe_2O_4$). In this analysis, EG denotes the ethylene glycol. Table 2 shows the validation of the present results of $-\theta'(0)$ with the existing results of Xu et al. [8] and Sandeep et al. [16]. We establish a good agreement with the existed results under the absence of R, M, S, ϕ and Pr = 1. This confirms the validity of our work.

The influence of magnetic field parameter (M) on the fluid velocity and temperature $(f'(\eta))$ and $\theta(\eta)$ are revealed in Figs. 2 and 3. It was detected that an enhancement in M



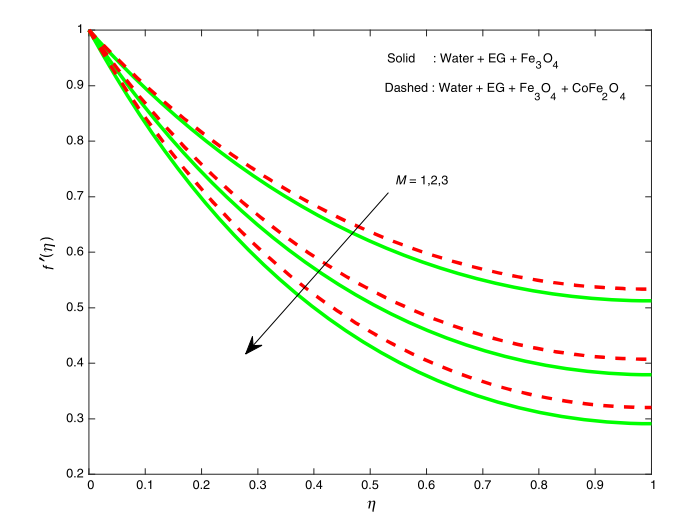


Fig. 2 Impact of magnetic field parameter on velocity

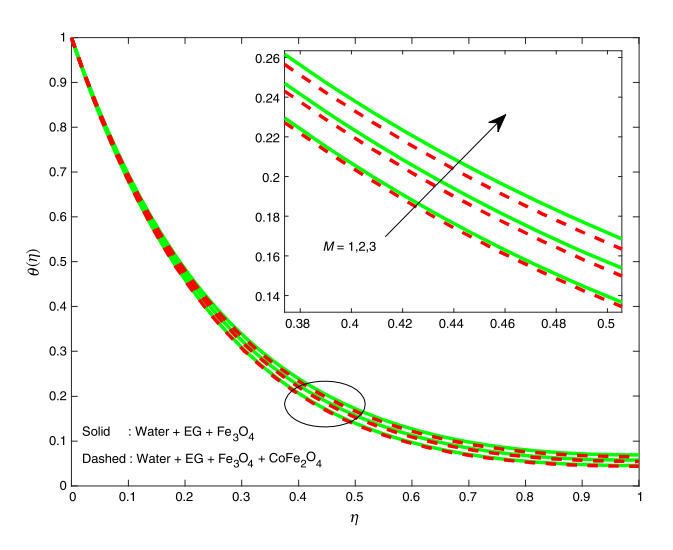


Fig. 3 Impact of magnetic field parameter on temperature

depreciates the curves of velocity in both the cases. But in the distribution of temperature, we originate that escalating value of M enhances the fluid temperature. A boost in the magnitude of M drops the thickness of the film consistently. This is because the accompanying ferroliquid yields a resistive type of force namely, Lorentz force. Along with this, some heat energy will be generated in the flow. It is found that the hybrid ferrofluid is highly influenced by drag force when compared to the individual ferrofluid.

Figures 4 and 5 explore the impact of film thickness parameter (λ) on the fluid velocity and temperature $(f'(\eta))$ and $\theta(\eta)$ of ferro- and hybrid ferrofluids, respectively. It is noticed that both the velocity and thermal fields decline with a large film thickness parameter. Physically, a rise in λ does not agree with the liquid to the motion. This may be the cause for decrease in the flow fields. It is also observed that the profiles of ferrofluid (water $+ EG + Fe_3O_4$) are

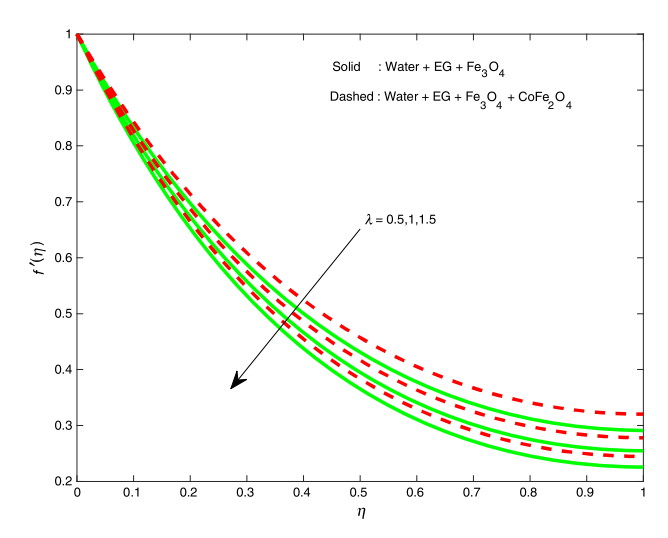


Fig. 4 Impact of film thickness parameter on velocity

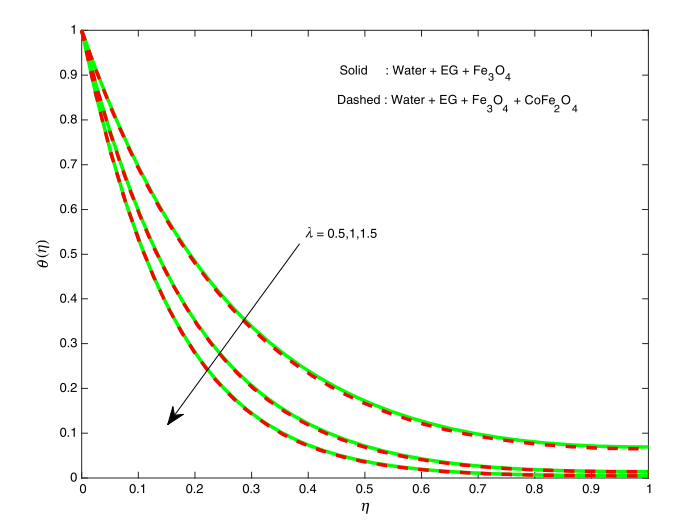


Fig. 5 Impact of film thickness parameter on temperature

more affected than that of the hybrid ferrofluid (water + EG + Fe₃O₄ +CoFe₂O₄) for λ .

The impact of radiation parameter (R) on the distribution of temperature ($\theta(\eta)$) is analyzed through Fig. 6. From the figure, it is noticed that the influence of R on $\theta(\eta)$ is increasing. It is familiar that the mechanism of radiation is the heat transference phenomenon which releases the energy via liquid particles such that some additional heat is produced in the flow. Hence, we detected an enrichment in the thermal field for larger R. We observed a motivating result that the curves of heat ($\theta(\eta)$) are more affected for water $+ EG + Fe_3O_4$ when compared that of water $+ EG + Fe_3O_4 + CoFe_2O_4$.

Figure 7 is depicted to deliberate the impact of S on the distribution of temperature. It is noticed that an enhancement in S depresses the fluid temperature. Since the unsteadiness parameter is controlled by both α and b, it is



2150 K. Anantha Kumar et al.

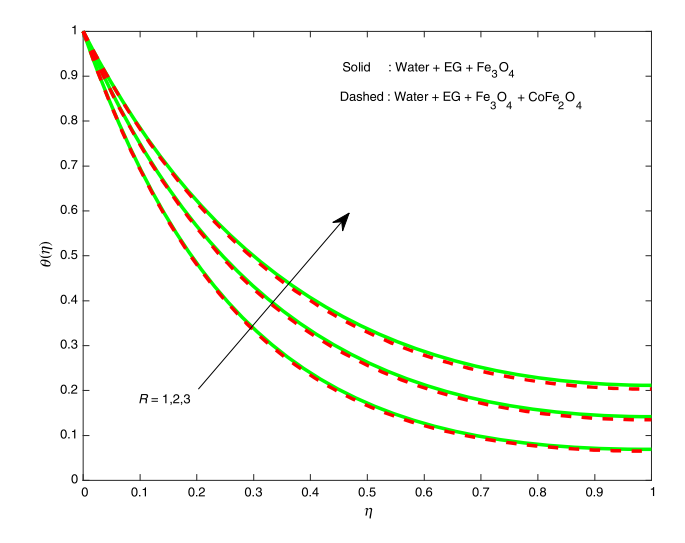


Fig. 6 Impact of radiation parameter on temperature

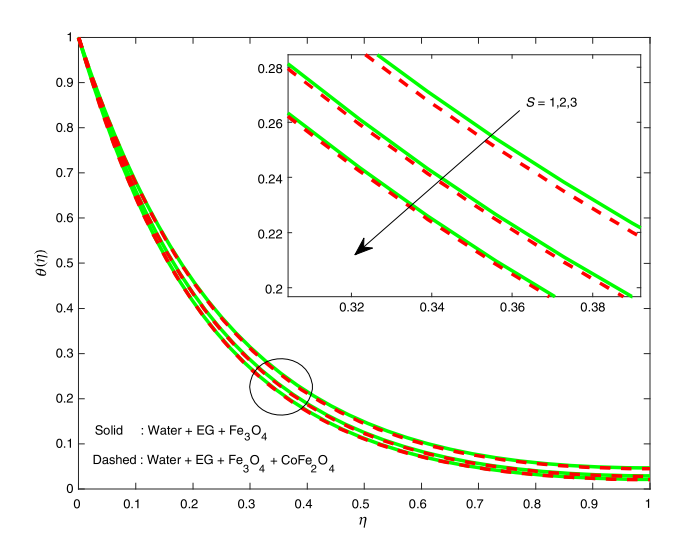


Fig. 7 Impact of unsteadiness parameter on temperature

familiar that the wall stretching velocity is precise significant for regulating the curves of velocity. Due to this, there is a fall in the thermal boundary layer is detected for larger *S*. Also, it is worth to mention that high temperature is noticed in the case of hybrid ferrofluid than that of ferrofluid.

The effect of uneven thermic sink/source parameters for the distribution of heat $(\theta(\eta))$ is revealed in Figs. 8 and 9. It was detected that boosting values of A^*,B^* result an enrichment in the fluid temperature. Basically, increasing values of irregular heat source/sink parameters acts as an agent to produce heat in the flow. Due to this, we observed that a rise in the fluid temperature for boosting the values of A^* and B^* . It is noticeable that the highest temperature is achieved in the case of water + EG + Fe₃O₄ when equated to the other.

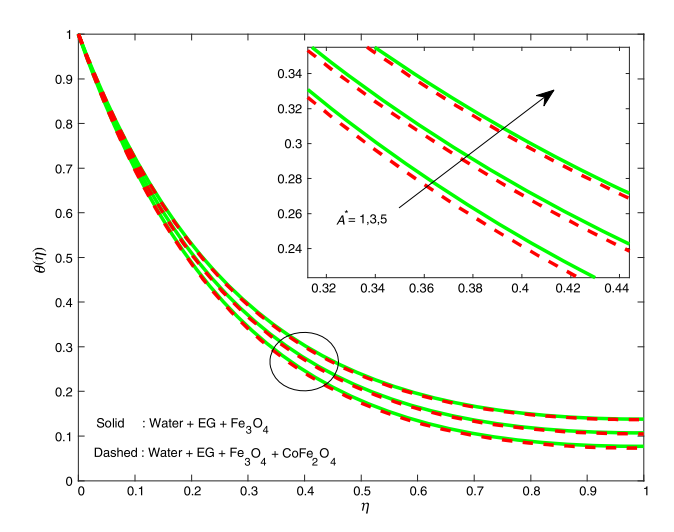


Fig. 8 Impact of non-uniform heat source/sink parameter on temperature

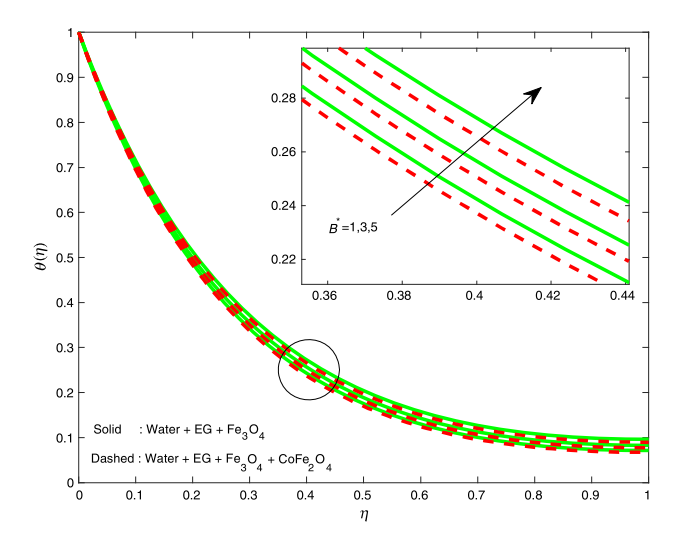


Fig. 9 Impact of non-uniform heat source/sink parameter on temperature

Figure 10 is illustrated to know the behavior of ϕ_1 and ϕ on the distribution of velocity of water + EG + Fe₃O₄ (ferrofluid) and water $+ EG + Fe_3O_4 + CoFe_2O_4$ (hybrid ferrofluid). It was detected that fluid velocity is an increasing function of volume fraction of hybrid ferrofluid, but an opposite result is noticed for the volume fraction of ferrofluids. It is interesting to note that high velocity is attained for ferrofluid than that of hybrid ferrofluid. Figure 11 is drawn to see the nature of both the volume fraction of ferrofluid (ϕ_1) and hybrid ferrofluids (ϕ) on the distribution of temperature on liquid film flow of H₂ O + EG + Fe₃O₄ and H₂O + EG + Fe₃O₄ + CoFe₂O₄. It was detected that fluid temperature is increasing the function of both the volume fraction of hybrid ferrofluid and ferrofluids (ϕ and ϕ_1). It is fascinating to mention that an enhancement in the thermal boundary layer thickness of

